Optical microcavities

Kerry J. Vahala

California Institute of Technology, Mail Stop 128-95, Pasadena, California 91125, USA (e-mail: vahala@caltech.edu)

Optical microcavities confine light to small volumes by resonant recirculation. Devices based on optical microcavities are already indispensable for a wide range of applications and studies. For example, microcavities made of active III–V semiconductor materials control laser emission spectra to enable long-distance transmission of data over optical fibres; they also ensure narrow spot-size laser read/write beams in CD and DVD players. In quantum optical devices, microcavities can coax atoms or quantum dots to emit spontaneous photons in a desired direction or can provide an environment where dissipative mechanisms such as spontaneous emission are overcome so that quantum entanglement of radiation and matter is possible. Applications of these remarkable devices are as diverse as their geometrical and resonant properties.

Like its acoustic analogue the tuning fork, the optical microcavity (or microresonator) has a size-dependent resonant frequency spectrum. Microscale volume ensures that resonant frequencies are more sparsely distributed throughout this spectrum than they are in a corresponding 'macroscale' resonator. An ideal cavity would confine light indefinitely (that is, without loss) and would have resonant frequencies at precise values. Deviation from this ideal condition is described by the cavity Q factor (which is proportional to the confinement time in units of the optical period). Q factor and microcavity volume (V) figure prominently in applications of these devices, and a summary of values typical for the devices discussed in this review is given in Table 1. In addition, representative examples of the three methods of confinement employed in microcavities are provided in Figs 1–3 (refs 1–7).

In this review, I consider four applications of optical microcavities: strong-coupling cavity quantum electrodynamics (QED), enhancement and suppression of spontaneous emission, novel sources, and dynamic filters in optical communication. These areas are just four of several possible, and many topics, such as soliton effects[8,9], chaos[10] and effects in quantum-well microcavities[11], will not be reviewed because of space limitations. Also, I will not review microcavity types in commercial semiconductor lasers because extensive texts and treaties on this subject already exist[12,13]. Even for the four applications discussed, there are by necessity omissions. Cavity QED, for example, is a vast topic, and selections have been made on the basis of their importance and for the interesting design limits they illustrate. I will provide a brief introduction to each area, then describe a few representative applications, their microcavity requirements, and the state-of-the-art for these devices, before outlining the challenges for the future.

Strong-coupling cavity QED

An electron transitions within an atom from an excited state to a ground state, emitting a photon into the continuum of radiation modes[14]. This irreversible behaviour is an example of weak coupling. If the same atom is inserted into a microcavity and if the strong-coupling conditions[15–17] described in Box 1 are satisfied, then the atom can interact coherently with a cavity mode for a meaningful time. This can take place even when the mode is initially in its vacuum state (ground state or state of lowest energy). Use of a weak optical probe reveals that the cavity's transmission spectrum is split by the presence of the atom into two distinct peaks, which correspond to eigenfrequencies of the quantum entangled atom-
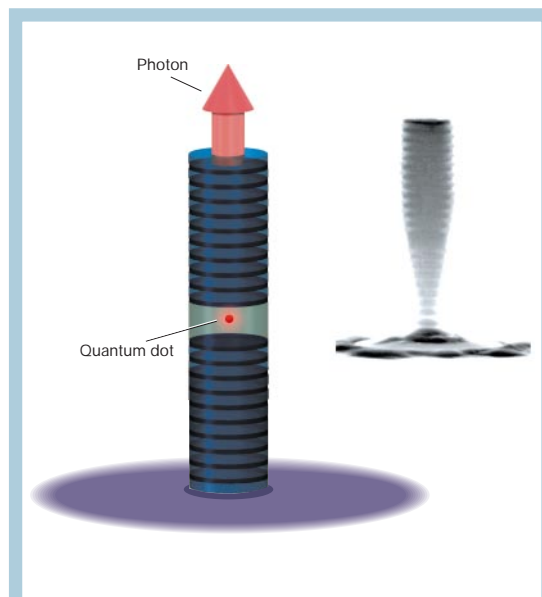

Figure 1 Micropost (or micropillar) cavities[1,2] have played a major role in recent applications of the Purcell effect to triggered, single-photon sources. They offer small cavity volume and relatively high Q, have an emission pattern that is well suited for coupling and manipulation of emitted photons[56] (for example, with optical fibres) and can incorporate quasi-atomic, quantum dots as emitters. In the rendering, Bragg mirrors[3] at the output (upper stack near arrow) and below provide one dimension of cavity confinement, whereas air-dielectric guiding provides lateral (in-the-plane) confinement. A single quantum dot is shown spontaneously emitting a photon that is subsequently directed via the Purcell effect through the cavity top. The inset shows a scanning electron micrograph of such a micropost cavity used in recent triggered single-photon source experiments. Inset micrograph courtesy of Y. Yamamoto[76] (Stanford University, CA).

cavity states (states that are not factorable into cavity and atom components)[18]. If the probe frequency is maintained at the cavity's original resonant frequency, then the entry of a single atom into the cavity can block transmission[19] (that is, the probe is reflected). In state-of-the-art systems, the resulting extreme sensitivity of transmission to the atom's position within the cavity is used to ascertain atomic centre-of-mass motion[20–22], such as the orbital motion of ultracold atoms entrained by their interaction with the cavity mode[21,22] (Fig. 4). In addition, such a cavity containing cold atoms exhibits extreme dispersive properties, which have
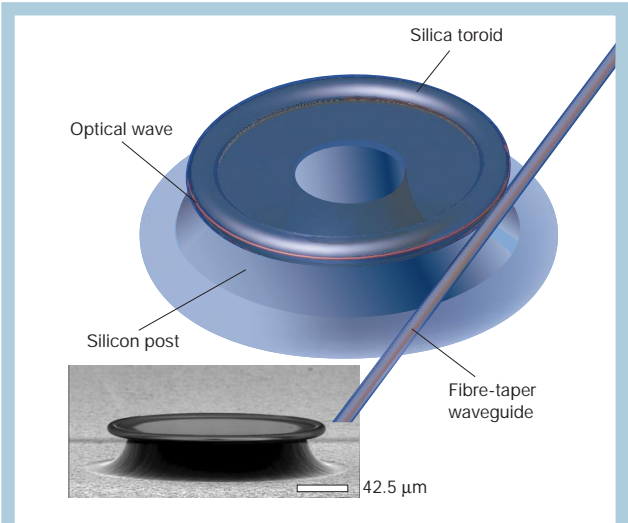
native measure of cavity perfection that does not include propagation effects within the cavity as does the Q factor, of 1.9×10^6 (ref. 26) has been obtained using these mirrors. Optimization of n_o and N_o, however, involves joint optimization of the mode volume and finesse (or Q). So, for example, the results cited above used a resonator with mode volume V=1.69×10^3 μm^3 and finesse of 4.8×10^5. A detailed review of the technological limits imposed by mirror technology in optimizing Fabry–Perot microcavities for strong-coupling studies has recently been performed[32].
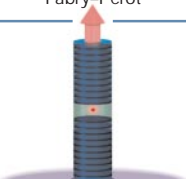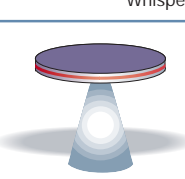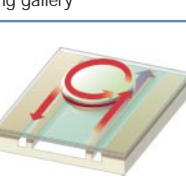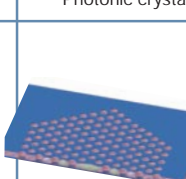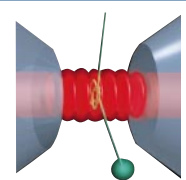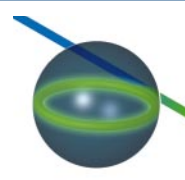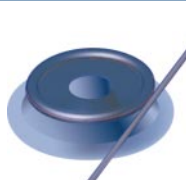
In addition to ultrahigh-finesse Fabry–Perot microcavities, the whispering gallery modes of silica and quartz microspheres have received considerable attention[27–29,33,34]. Whispering gallery resonators are typically dielectric spherical structures in which waves are confined by 'continuous total internal reflection'. Silica microspheres, which are robust ultrahigh-Q microresonators, were first studied by Braginsky and Ilchencko[35]. Spheres feature an atomic-like mode spectrum in which high ℓ number (principal angular index or optical mode) and low radial number modes execute orbits near the sphere's surface[33] (Fig. 5). Excellent surface finish is crucial for maximizing Q, and the formation of spheres through surface tension (that is, as a molten droplet) provides a near atomically smooth surface (with only a few nanometres or less of surface roughness[28,29]). The bulk optical loss from silica is also exceptionally low and record Q factors[28,29] of 8×10^9 (and finesse[29] of 2.3×10^6) have been obtained. For these measurements, dependence of Q on sphere diameter is consistent with Q being limited by losses of surface roughness[29]. Also, a time dependency for the measured Q was observed and is believed to result from water adsorption and formation of OH groups at the sphere's surface[28,34]. For diameters below 20 μm in silica spheres, radiation leakage becomes a significant factor in determining Q[31]. The lowest order radial modes (in terms of nodes) with $m=\ell$[31] are minimal volume, equatorial ring orbits (see Fig. 5) and are best suited for cavity QED. Experimental work has demonstrated strong coupling in this system[34], and recent modelling[31] shows that substantial improvements in strong coupling are possible using spheres with reduced diameters.

Microcavities based on photonic crystals (Fig. 3) can provide extremely small mode volumes[7], and donor-mode cavity geometries (in which a small additional hole is drilled within the design of Fig. 3) have been modelled with a neutral atom suspended within the hole[30]. Strong coupling is theoretically feasible; however, at present, Q values in fabricated structures are well below the theoretical optima.

For the purposes of optical probing/output-coupling, Fabry–Perot cavities enable direct 'endfire' coupling along the cavity axis. Whispering gallery modes, however, must be phase matched[36],

Figure 2 Rendering of an ultrahigh-Q microtoroid resonator[6]. An optical wave, shown in red, is coupled from a fibre-taper waveguide and subsequently guided within and along the periphery of the microtoroid in a whispering gallery mode, which is named after its acoustic equivalent[5]. Whispering gallery microcavities can be found in several geometries including spheres (see Fig. 5), disks (see Fig. 6) and rings (inset to Fig. 6). Inset: A scanning electron micrograph of a microtoroid resonator consisting of a thin silica layer upon a silicon post and substrate. The device has a diameter of 120 μm and exhibits a Q factor in excess of 100 million. The smooth exterior toroid surface is the result of the toroid going through a molten state during its fabrication. Inset micrograph courtesy of D. Armani[6].

recently been observed[23]. These measurements, as well as applications of cavity QED to quantum information studies, have recently been reviewed elsewhere[24,25].

Efforts to increase strong-coupling effects (as measured by reductions in saturation photon number, n_o, and critical atom number, N_o (see Box 1)) have provided much impetus for research into ultrahigh-Q, small-volume resonant cavities[17,26–30]. Both n_o and N_o have been lowered from near unity levels in the earliest demonstrations of single-atom vacuum Rabi splitting at optical frequencies to recent levels of $n_o = 2.82 \times 10^{-4}$ and $N_o = 6.1 \times 10^{-3}$ (refs 21,31). Microcavities in these experiments feature Fabry–Perot-style resonators (an optical resonator in which feedback is accomplished using two mirrors) with ultrahigh reflectance mirror technology[26]. A cavity finesse, an alter-

Table 1

The microcavities are organized by column according to the confinement method used and by row according to high Q and ultrahigh Q. Small mode volume and ultrasmall mode volume are other possible classifications that are somewhat complementary to this scheme. Representative, measured Qs and Vs are given and have been taken from the following cited references. Upper row: micropost[48], microdisk[52], semiconductor[103], polymer[104] add/drop filter, photonic crystal cavity[62]. Lower row: Fabry-Perot bulk optical cavity[21,31], microsphere[29], microtoroid[6]. n is the material refractive index, and, V, if not indicated, was not available. Microsphere volume V was inferred using the diameter noted in the cited reference and finesse (F) is given for the ultrahigh-Q Fabry–Perot as opposed to Q. Two Q values are cited for the add/drop filter: one for a polymer design, Q_{Poly}, and the second for a III–V semiconductor design, $Q_{III–V}$.

|	Fabry–Perot	Whispering gallery		Photonic crystal
High Q	Q: 2,000 V: 5 $(\lambda/n)^3$	Q: 12,000 V: 6 $(\lambda/n)^3$	$Q_{III–V}$: 7,000 Q_{Poly}: 1.3x10^5	Q: 13,000 V: 1.2 $(\lambda/n)^3$
Ultrahigh Q	F: 4.8×10^5 V: 1,690 μm^3	Q: 8×10^9 V: 3,000 μm^3	Q: 10^8	

Box 1
Strong coupling

An atom, initially in the excited state of a dipole transition, enters a lossless microcavity of volume V. A single mode of the cavity, in its ground state, is resonant with the transition. The atom and 'vacuum field' couple, which results in a quantum of energy shifting back and forth between the atom and the mode at the vacuum Rabi frequency. The interaction strength of atom and cavity mode is linear in the field and hence smaller cavity volumes concentrate the vacuum field of the mode, producing larger Rabi frequencies. This fundamental dynamic of the atom–field system is reversible as long as the system is isolated. In reality the cavity will have a finite photon lifetime (finite Q) that will limit, perhaps even prevent, Rabi oscillations by allowing the energy to leak irreversibly into the continuum. Likewise, the atomic transition will couple to continuum radiation modes and thereby experience spontaneous decay of its population as well as polarization dephasing. Strongly coupled systems are those in which the Rabi dynamic can exist, even if only briefly, despite the reality of dissipation. Strong coupling occurs when the atom–field coupling strength, g (which is half the Rabi frequency), is faster than any underlying dissipative rate and larger than $1/T$ where T is the interaction time[17]. Under conditions of strong coupling, weak optical probing near the microcavity resonant frequency reveals two spectral transmission peaks (where only one existed before) giving the energies of new eigen states, which are now entangled states of the atom and cavity field. Given modal and atomic dissipation, the degree to which the atom and cavity mode are strongly coupled can be quantified by defining a saturation photon number (n_o) and critical atom number (N_o). These quantities are, by necessity, functions of parameters describing both the reversible dynamic and the various decay rates[17],

$$n_o \propto \frac{\gamma_\perp \gamma_\parallel}{g^2} \propto V \qquad\qquad N_o \propto \frac{\gamma_\perp}{\tau g^2} \propto \frac{V}{Q}$$

where ($\gamma_\parallel$, $\gamma_\perp$) are the atomic dissipation rates (population relaxation and atomic dephasing, respectively) and τ is the cavity lifetime. In 1992, unity n_o and N_o were demonstrated at optical frequencies[18]. Recently, state-of-the-art, strongly coupled systems have produced n_o and N_o values that are much less than unity, reflecting a fundamental Rabi dynamic that exists over many cycles. For reviews of strong coupling and its application to cavity QED see refs 17,25,46,120.
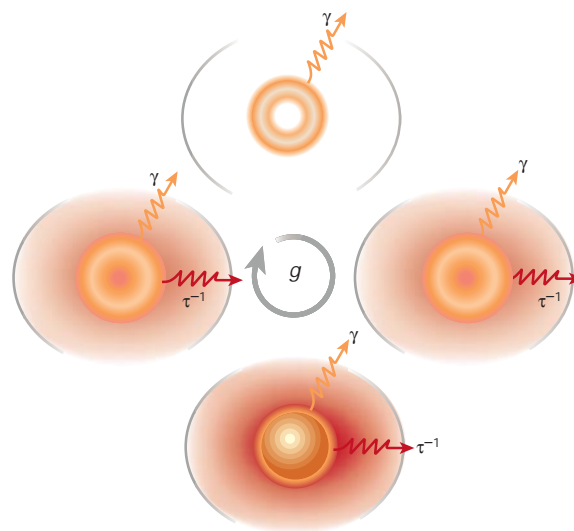
Box 1 Figure Vacuum Rabi oscillation. An excited atom is introduced into the cavity (top) and undergoes vacuum Rabi oscillation mediated by the atom-field coupling strength, g, resulting in one quantum being added to the mode (shown in red) (bottom). Dissipation mechanisms are also illustrated. γ is the atomic damping rate and τ is the cavity lifetime.

which is typically achieved using total internal reflection from the back face of a prism. Other coupling methods have also been demonstrated[37–40]. For many applications of cavity QED, such as in quantum information studies, parasitic loss in coupling to and from microresonators will figure prominently. A fibre-optic cable is considered a likely medium over which to transport quantum information[41]. In this regard, fibre-optic tapers (see Fig. 5) provide ultralow loss, direct coupling to ultrahigh-Q spheres[42] and have been proposed as a means to couple quantum states to or from a resonator onto a fibre[42,43]. Also, the recent demonstration of a fibre-taper-coupled ultrahigh-Q microtoroid-on-a-chip[6] (see Fig. 2) enables integration of wafer-based functions with ultralow-loss fibre-coupled quantum devices.

Enhancement and suppression of spontaneous emission

Weak coupling results when dissipation overwhelms the fundamental Rabi dynamic. The control of spontaneous emission through the Purcell effect[44] in this regime has become an important application of microcavities[45]. Because all cavities exhibit loss at some level, cavity modes are, more rigorously, quasi modes, and, in the strictest sense, the spectral–lineshape function of a 'discrete' mode is proportional to a continuum density of modes (DM) function (ref. 4, chapter 1, and references therein). Applications of the Purcell effect make use of this duality by, on the one hand, using local enhancement of the continuum DM function to influence spontaneous emission, while, on the other, using the quasi mode of the resonator as the target of the emission process (see Box 2 for further discussion of this and the complementary effect, spontaneous-emission suppression). Thus, atomic decay rates are not only speeded-up but are also made direc-

tional. Reviews of this mechanism both at optical and at microwave frequencies appear in ref. 4 (chapter 2) and ref. 46.

The ability to create InAs quantum dots that have excellent luminescent properties[47] within III–V semiconductors was a turning point in the recent history of the Purcell effect. As noted by Gerard[1], these structures can act as a local probe of the field within a III–V microcavity and can also efficiently capture and then confine electrons and holes, making them less susceptible to the semiconductor surface effects that occur when cavity dimension decreases. Quantum dots are also well suited to the study of the Purcell effect in semiconductors, because, unlike bulk or quantum-well media, individual quantum dots exhibit a relatively narrow spectral lineshape that fits within a high-Q microcavity mode[48,49].

Using quantum-dot-loaded micropost[1,3] (or micropillar) cavities, such as the one shown in Fig. 1, with Qs of 2,000 (1 μm diameter posts), Gerard and coworkers showed a five-fold Purcell enhancement[48,50]. Spontaneous emission suppression was later verified in similar structures using a metallic sidewall coating to exclude transverse continuum modes[51]. Purcell enhancement of emission from a single quantum dot within a micropost was later demonstrated[2]. In addition to microposts, microdisk cavities incorporating quantum dots support modes with Qs in the range of 10,000–17,000[52,53], and Purcell enhancement has been measured[54] up to 15-fold[55] in these structures. Measured Purcell factors are influenced by radial spatial averaging, which occurs over an ensemble of resonant emitters[48,56], and estimated Purcell factors based on Q measurement and cavity volume estimates are typically much higher. Using Q measurement alone, a Purcell factor of 32 for microposts[50] and a factor of

---

Box 2
Purcell effect

A two level system will decay spontaneously by interaction with a vacuum continuum at a rate proportional to the spectral density of modes per volume evaluated at the transition frequency. Within a cavity, the density of modes is modified and large swings in its amplitude can occur. From the viewpoint of cavity modes (which in the presence of dissipation must be viewed as quasi modes (ref. 4, chapter 1)), the maximal density of modes occurs at the quasi-mode resonant frequencies and can greatly exceed the corresponding free-space density. Historically, Purcell[44] arrived at this conclusion by noting that a single (quasi) mode occupies a spectral bandwidth ν/Q within a cavity of volume V. Normalizing a resulting cavity-enhanced mode density per unit volume to the mode density of free space yields the 'Purcell' spontaneous emission enhancement factor[44,46].

$$P = \frac{3}{4\pi^2}\left(\frac{\lambda}{n}\right)^3 \frac{Q}{V}$$

where refractive index, n, is a modern addition to this expression to account for emission within dielectrics[55]. An atom whose transition falls within the mode linewidth will experience an enhancement to its spontaneous decay rate given by the Purcell factor. More significantly, because the enhancement comes about from coupling to only those continuum modes that make up the corresponding quasi-mode of the resonator, the spontaneous emission is directed to this quasi mode[88] and has great utility with regard to coupling spontaneous power.

In spectral locations that are intermediate to modal resonance frequencies, the density of the modes can fall well below the density in free space. With proper cavity design and for operation at these off-resonance frequencies, spontaneous decay can be suppressed[4,46,58]. Rigorous developments of Purcell's physical model have been

presented on the basis of calculation of the continuum mode density (ref. 4, chapters 1 and 2 and references therein).

Design of microcavities for observation of the Purcell effect must take account of the corresponding atomic (or atom-like) transition characteristics. Use of a small microcavity volume is important because enhancements driven by manipulation of Q alone are limited by the spectral width of the transition. Likewise, all other things being equal, narrow, atomic transitions can be Purcell-enhanced more as a higher Q becomes possible. It is for this reason that individual quantum dots, with their relatively narrow transition widths (compared with bulk semiconductors), are playing a significant role in this field[49] (see Fig. 1).
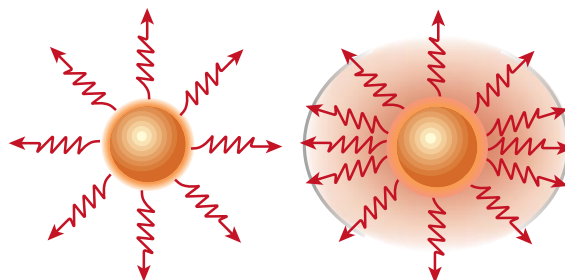
Box 2 Figure Purcell enhancement of spontaneous emission. Weak coupling to a cavity mode will enhance the spontaneous rate of emission by increasing the local density of modes (right) compared with their density in free space (left).

---

190 for 2 μm diameter microdisks[52] have been inferred. Q factors as high as 10,000 with corresponding mode volumes of 1.6 $(\lambda/n)^3$ have been predicted to exist in optimized micropost cavities[57]. A post diameter of 0.5 μm with an improved Q factor of 4,800 yields a Purcell factor of 147[56,57].

Since Yablonovitch first proposed using a photonic crystal for spontaneous emission suppression[58], much attention has been directed to photonic bandgap microcavities[59,60]. As noted earlier, photonic-crystal defect microcavities can provide extremely small mode volumes[7], and large theoretical Q values have been predicted for certain designs[30,61]. Recently, a Q of 4,000 for an H2 (seven holes removed to form the hexagon) defect cavity[59] and a Q of 13,000[62] for a donor-mode cavity (calculated mode volume of 1.2 $(\lambda/n)^3$) were reported. Purcell enhancement has also been studied in this system[60,63].

Controlling the emission of single photons has been a priority for quantum encryption systems[64]. Single-photon sources, which are required in these systems, are a recent application of the Purcell effect in quantum-dot microcavities (see Fig. 1). Quantum dots are quasi-atomic systems and hence share many properties with atoms. For example, emission from a single atom or molecule and from quantum dots[67] exhibits non-classical photon anti-bunching behaviour, because, upon emission, an interval must pass in order for the atom to be re-excited and to emit a photon[65,66]. This behaviour in quantum dots has been adapted to generate triggered single photons[68–71]. Leading up to this application, triggered single-photon emission using photo-pumped, single-molecule systems was demonstrated[72,73]. However, quantum-dot single-photon sources, which are compact and potentially electrically pumped, are very appealing for many of the same reasons that semiconductor lasers are so compelling in communications. Unlike lasers, however, the useful emission in these new quantum sources is a spontaneous photon; therefore, stimulated emission cannot be relied upon to direct

power into a single cavity mode (a necessity for efficient coupling to optical fibres). Instead, the Purcell effect is applied to improve coupling[55]. Both microdisk[68] and micropost-based devices[74–76] have been demonstrated. Significantly, a single photon source that is an electrically pumped single quantum dot has recently been demonstrated[77]. An
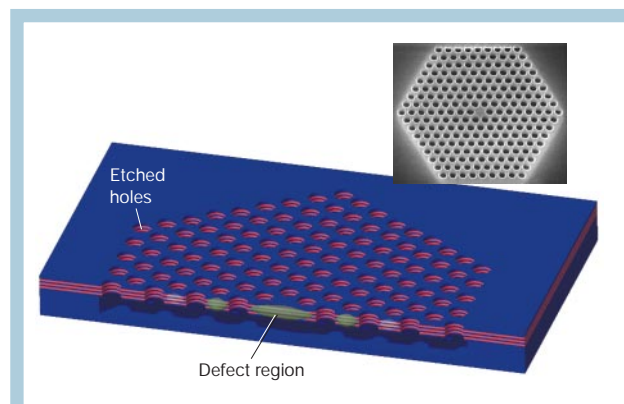

Figure 3 Cross-sectional illustration of a photonic crystal defect microcavity laser. The microcavity is formed by dry etching a hexagonal array of holes and subsequent selective etch of an interior region, creating a thin membrane. One hole is left unetched creating a 'defect' in the array and therefore a defect mode in the optical spectrum. The mode (illustrated in green) is confined to the interior of the array by Bragg reflection in the plane and conventional waveguiding in the vertical direction. Also, shown in pink are quantum wells that upon photo pumping provide the amplification necessary for laser oscillation[7]. Inset: Scanning electron micrograph of a photonic crystal defect microcavity laser. Micrograph is courtesy of O. Painter and A. Scherer (Caltech, CA).
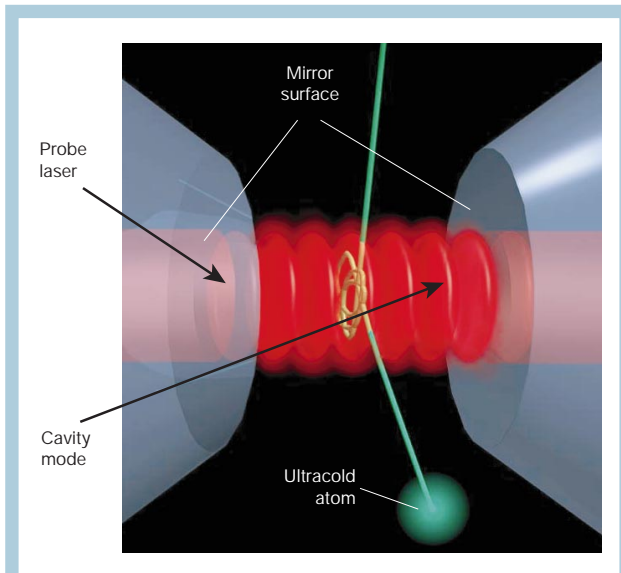
Figure 4 If the coupling energy $\hbar g$ in a strongly coupled system exceeds the thermal energy of the atom, then the atomic centre of mass motion will be altered by interaction with the vacuum cavity mode. In recent experiments[21,22], ultracold atoms have been produced to satisfy this condition, resulting in atomic motion that is entrained for substantial periods of time by cavity QED coupling. In this figure, an ultracold atom is entrained in an orbital motion before escaping. Because the coupling energy depends on the amplitude of the vacuum cavity field near the atom, optical transmission probing of the cavity during the atomic entrainment acts as an ultrasensitive measure of atomic location. Figure used with permission of H. J. Kimble (Caltech, CA).

important next step will be to combine this feature with a microcavity equipped for significant Purcell enhancement.

Novel sources

The pursuit of efficient and compact laser sources that offer enhanced functionality or that provide insight into microcavity physics has inspired a large body of microcavity research. Lasing has been demonstrated in droplets[78,79], silica[38,80] and polystyrene spheres[81], semiconductor microdisks[52,82,83], micropillars[3] (vertical cavities[84]) and photonic crystal cavities[7]. Small cavity volumes and high Q have allowed the production of submicrowatt optical pump thresholds[85] in microspheres and microamp-scale current thresholds in semiconductor lasers[86,87]. With the advent of multi-wavelength communications systems[12], tunable and compact sources have taken on an increased importance. In addition, interest in the Purcell effect and more efficient lasers has focused attention on threshold control[88] and also on the concept of threshold[89]. Lasers[90] that operate like micro-masers[15,46] have also been studied.

A development of practical importance is the use of lateral oxidation in vertical cavity lasers[84]. These lasers have a lateral oxide aperture that is normal to the cavity axis, which creates lateral mode confinement and concentrates pumping current at the optical gain region, thereby making the device very efficient[86,87]. Cavity enhancement effects have also been observed in versions of these devices containing quantum dots[91].

Sources that use a nonlinearly stimulated process to achieve laser action represent another class of device. Resonant recirculation of weak input signals within ultrahigh-Q, small-mode–volume resonators will produce enormous modal field intensities and thereby lower the threshold for nonlinear phenomena[35]. For a given coupled, input power, P_{in}, the circulating intensity within the resonator is given by $I = P_{in}(\lambda/2\pi n)(Q/V)$ where n is the group index. For a cavity Q of 100 million and a mode volume of 500 μm^3 (both obtainable in spheres roughly 40 μm in diameter[31,43]) the circulating intensity

exceeds 1 GWatt/cm^2 with less than 1 mW of coupled input power. Observation of stimulated Raman scattering[92,93], multi-order Stokes emission[94], stimulated Brillouin scattering[95] and many other nonlinear effects were first studied in microdroplets by Chang[92] and by Campillo (ref. 4, chapter 5, and references therein). The Kerr effect has also been observed by Treussart et al. in ultrahigh-Q silica microspheres[96] at microwatt input power levels. More recently, efficient solid-state Raman laser sources using fibre-coupled[42] ultrahigh-Q microspheres have been demonstrated, and they produced record-low-threshold pump powers of 65 μW (ref. 43) (see Fig. 5). Raman sources can be used to extend the wavelength range of conventional lasers into difficult-to-access bands.

Dynamic filters in optical communications

During the past decade, wavelength division multiplexed (WDM) lightwave systems have been deployed in long-distance transmission to take better advantage of the vast bandwidth available in an optical fibre[97]. Beyond providing additional bandwidth, wavelength, used as a dynamic parameter, can enhance network performance[98]. With attention turned towards future system needs, there has been interest in devices that enable new filtering and switching functions[99].

A microcavity filter that has received considerable attention is one that enables resonant transfer of optical power between two waveguides. In its simplest form, it consists of a single whispering gallery microresonator sandwiched between two single-mode waveguides (Fig. 6). As a passive filter, this structure can perform a function called channel add/drop in which a single channel is 'dropped' with high extinction from a first waveguide and coupled with low loss to a second waveguide. In practice, this coupling should take place with high selectivity because other wavelength channels will be present on the input waveguide. Other versions of this device (that are not based on a microresonator) are also being investigated[99–101]; however, the microresonator version is attractive because of its small size and potential for high-density integration on a wafer[102]. If the whispering gallery resonator is made active by addition of an electrically controllable refractive index, then the add/drop function is dynamic and provides control of the resonant wavelength for tuning[103], ultrafast modulation[104] or switching. Alternatively, introducing a controlled loss within the resonator enables switching-off of the coupling[105–107]. Arrays of these devices on a common sub-
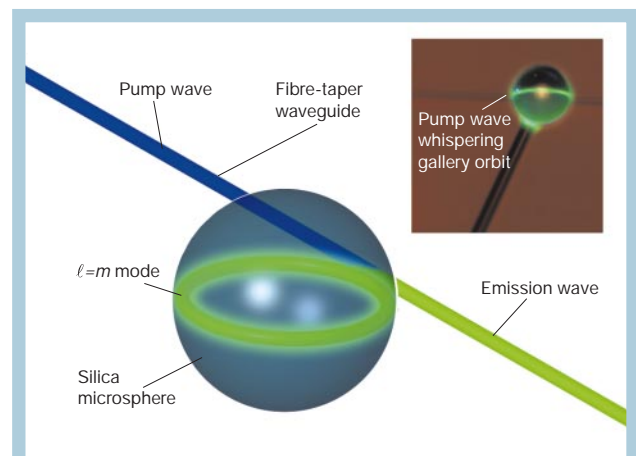

Figure 5 Illustration of a silica microsphere whispering gallery resonator. The green orbit is a $\ell=m$ mode entrained at the sphere's surface. Also shown is a fibre taper waveguide used for power coupling to and from the resonator. In the figure, a blue pump wave induces a circulating intensity within the sphere that is sufficient to induce laser oscillation (green emission wave). Inset: Photomicrograph showing a doped microsphere (the glass sphere contains a rare earth). The green emission in this case traces the pump wave whispering gallery orbit. The inset micrograph was provided by M. Cai.
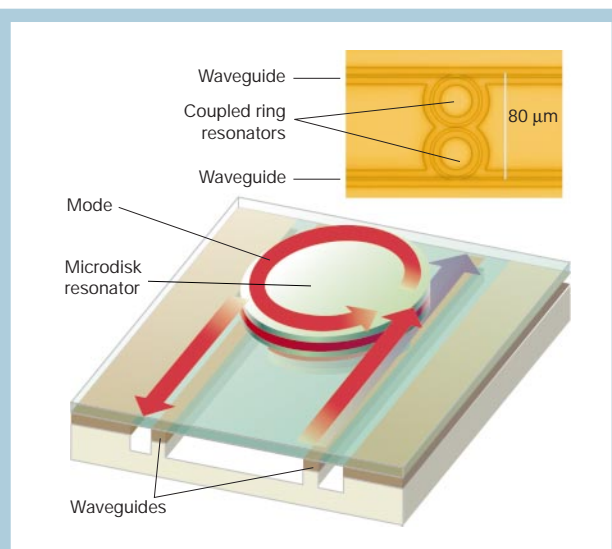
Figure 6 Illustration of a microcavity add/drop filter in which two buried waveguides (shown in brown) are vertically coupled to a disk whispering gallery resonator. This structure is fabricated by first creating the waveguides through a process of lithography and etching and then wafer bonding an initially mechanically separate, second wafer containing layers that ultimately become the microresonator. After wafer bonding, the substrate is removed from the second wafer, and lithography and etching are applied to create the microdisk. Critical gaps that control field-coupling strengths between waveguides and the microresonator are thereby determined by thin-film crystal growth methods as opposed to lithography and etching as is the case in side-coupled structures. As shown, a red input channel is resonant with a mode of the disk and is subsequently coupled through to the second waveguide. A blue channel that is non-resonant is also shown. The channel add function is not illustrated; however, it results from coupling power into the other port of the drop waveguide with subsequent resonant coupling to the input waveguide along the indicated direction of signal flow. This device can be made dynamic by inclusion of electrically controllable loss or refractive layers within the resonator. Low-loss coupling and high drop extinction require the microdisk to have an intrinsic Q factor, Q_0, that is substantially larger than its Q factor under conditions of waveguide loading, Q_L. Furthermore, efficient coupling requires waveguide loading to be balanced, such that field coupling between the disk and each waveguide is nearly equal. Q_L is then determined by the requisite information bandwidth, B, with $B < \nu/Q_L$ required for proper information transfer. This schematic is based on one by P. D. Dapkus[103]. The inset is a photomicrograph of a ring-resonator add/drop filter provided by Brent Little (Little Optics). The device shown is a 'second order' design containing a pair of coupled ring resonators. The waveguides (top and bottom) feature 'vertical coupling' to the resonators, providing excellent coupling control.

strate[108,109] or interconnected by a fibre could one day be used to perform complex functions within the context of WDM.

Many versions of this basic design have been demonstrated, including monolithic III–V[110], silica[111] and polymer-based devices[104]. Arrays have also been fabricated to explore issues associated with fabrication tolerance and post-process trimming[102]. The major challenge for fabrication of these devices is ensuring control and reproducibility of waveguide-to-resonator coupling and resonator dimensions. One approach to obtaining better fabrication control of coupling is to use so-called vertical coupling structures (coupling regions that are defined primarily by layer thickness as opposed to lithography)[104,106,111].

Another challenge for fabrication concerns the spectral shape and filter roll-off characteristics of these devices. Spectral response functions with roll-offs that are steeper than are possible using a simple Lorentzian (single pole) filter response are necessary for concatenation of components in networks[112]. Designs for such multi-pole filters based on coupled resonators[113] have been proposed, and several devices have been demonstrated[114,115]. Active frequency control[103] or

UV trimming of device refractive index[102] could be required to offset fabrication-induced variances in critical resonator dimensions.

Future directions

We have reviewed four broad application areas of optical microcavities and highlighted several microcavity designs for each (see Table 1). Impressive results have been achieved in all areas. Substantial, additional gains are possible in quantum optical applications with continued improvement in microfabrication techniques and with implementation of new low-loss designs. Triggered, single photon sources will benefit from higher Purcell factors for improved fibre coupling, and miniaturization to the submicrometre scale of cavity QED devices (using either strong or weak coupling) is feasible. Also, the emergence of new ultrahigh-Q, wafer-based geometries should provide a platform for strong-coupling studies that combine both laboratory-on-chip functions and efficient coupling to optical fibres. Technological applications such as the dynamic add/drop device will provide better control and reproducibility of filter characteristics in designs that are increasingly complex.

One other area that deserves special note is that of biological and chemical sensing. Optical sensors that use evanescent field coupling have been developed[116,117]; however, high-Q optical microcavities, as a sensor transducer, offer the potential to greatly enhance detection sensitivity[39]. Recently, sensors based on both monolithic[118] and microsphere[119] whispering gallery transducers have been demonstrated. It seems likely that this will become an important application area for these devices. Likewise, the broad technological impact that resonant devices have had at acoustic, radio and microwave frequencies suggests that many other applications for these devices will emerge in the optical domain. ☐

1. Gerard, J. M. *et al.* Quantum boxes as active probes for photonic microstructures: The pillar microcavity case. *Appl. Phys. Lett.* **69,** 449–451 (1996).
2. Solomon, G. S., Pelton, M. & Yamamoto, Y. Modification of spontaneous emission of a single quantum dot. *Phys. Status Solidi* **178,** 341–344 (2000).
3. Jewell, J. L. *et al.* Lasing characteristics of GaAs microresonators. *Appl. Phys. Lett.* **54,** 1400–1402 (1989).
4. Chang, R. K. (ed.) *Optical Processes in Microcavities* (World Scientific, Singapore, 1996).
5. Rayleigh, L. in *Scientific Papers* 617–620 (Cambridge Univ., Cambridge, 1912).
6. Armani, D. K., Kippenberg, T. J., Spillane, S. M. & Vahala, K. J. Ultra-high-Q toroid microcavity on a chip. *Nature* **421,** 925–928 (2003).
7. Painter, O. *et al.* Two-dimensional photonic band-gap defect mode laser. *Science* **284,** 1819–1821 (1999).
8. Taranenko, V. B. & Weiss, C. O. Spatial solitons in semiconductor microresonators. *IEEE J. Select. Top. Quantum Elect.* **8,** 488–496 (2002).
9. Barland, S. *et al.* Cavity solitons as pixels in semiconductor microcavities. *Nature* **419,** 699–702 (2002).
10. Stone, A. D. Wave-chaotic optical resonators and lasers. *Physica Scripta* **T90,** 248 -262 (2001).
11. Khitrova, G., Gibbs, H. M., Jahnke, F., Kira, M. & Koch, S. W. Nonlinear optics of normal-mode-coupling semiconductor microcavities. *Rev. Mod. Phys.* **71,** 1591–1639 (1999).
12. Brinkman, W. F., Koch, T. L., Lang, D. V. & Wilt, D. P. The lasers behind the communications revolution. *Bell Labs Tech. J.* **5,** 150–167 (2000).
13. Coldren, L. A. & Corzine, S. W. *Diode Lasers and Photonic Integrated Circuits* (Wiley, New York, 1995).
14. Yariv, A. *Quantum Electronics* (Wiley, New York, 1989).
15. Berman, P. R. (ed.) *Cavity Quantum Electrodynamics* (Academic Press, New York, 1993).
16. Haroche, S. Entanglement, mesoscopic superpositions and decoherence studies with atoms and photons in a cavity. *Physica Scripta* **T76,** 159–164 (1998).
17. Kimble, H. J. Strong interactions of single atoms and photons in cavity QED. *Physica Scripta* **T76,** 127–137 (1998).
18. Thompson, R. J., Rempe, G. & Kimble, H. J. Observation of normal-mode splitting for an atom in an optical cavity. *Phys. Rev. Lett.* **68,** 1132–1135 (1992).
19. Mabuchi, H., Turchette, Q. A., Chapman, M. S. & Kimble, H. J. Real-time detection of individual atoms falling through a high- finesse optical cavity. *Opt. Lett.* **21,** 1393–1395 (1996).
20. Rempe, G. One-atom in an optical cavity - spatial-resolution beyond the standard diffraction limit. *Appl. Phys. B* **60,** 233–237 (1995).
21. Hood, C. J., Lynn, T. W., Doherty, A. C., Parkins, A. S. & Kimble, H. J. The atom-cavity microscope: Single atoms bound in orbit by single photons. *Science* **287,** 1447–1453 (2000).
22. Pinkse, P. W. H., Fischer, T., Maunz, P. & Rempe, G. Trapping an atom with single photons. *Nature* **404,** 365–368 (2000).
23. Shimizu, Y. *et al.* Control of light pulse propagation with only a few cold atoms in a high-finesse microcavity. *Phys. Rev. Lett.* **89,** 233001 (2002).
24. Mabuchi, H. & Doherty, A. C. Cavity quantum electrodynamics: Coherence in context. *Science* **298,** 1372–1377 (2002).
25. Raimond, J. M., Brune, M. & Haroche, S. Colloquium: Manipulating quantum entanglement with atoms and photons in a cavity. *Rev. Mod. Phys.* **73,** 565–582 (2001).
26. Rempe, G., Thompson, R. J., Kimble, H. J. & Lalezari, R. Measurement of ultralow losses in an optical interferometer. *Opt. Lett.* **17,** 363–365 (1992).

27. LefevreSeguin, V. & Haroche, S. Towards cavity-QED experiments with silica microspheres. *Mat. Sci. Eng. B* **48**, 53–58 (1997).

28. Gorodetsky, M. L., Savchenkov, A. A. & Ilchenko, V. S. Ultimate Q of optical microsphere resonators. *Opt. Lett.* **21**, 453–455 (1996).

29. Vernooy, D. W., Ilchenko, V. S., Mabuchi, H., Streed, E. W. & Kimble, H. J. High-Q measurements of fused-silica microspheres in the near infrared. *Opt. Lett.* **23**, 247–249 (1998).

30. Vuckovic, J., Loncar, M., Mabuchi, H. & Scherer, A. Design of photonic crystal microcavities for cavity QED. *Phys. Rev. E* **6501**, 016608 (2002).

31. Buck, J. R. and Kimble, H. J. Optimal sizes of dielectric microspheres for cavity QED with strong coupling. *Phys. Rev. A* 033806 (2003).

32. Hood, C. J., Kimble, H. J. & Ye, J. Characterization of high-finesse mirrors: Loss, phase shifts, and mode structure in an optical cavity. *Phys. Rev. A* **6403**, 033804 (2001).

33. Knight, J. C. *et al.* Mapping whispering-gallery modes in microspheres with a near-field probe. *Opt. Lett.* **20**, 1515–1517 (1995).

34. Vernooy, D. W., Furusawa, A., Georgiades, N. P., Ilchenko, V. S. & Kimble, H. J. Cavity QED with high-Q whispering gallery modes. *Phys. Rev. A* **57**, R2293–R2296 (1998).

35. Braginsky, V. B., Gorodetsky, M. L. & Ilchenko, V. S. Quality-factor and nonlinear properties of optical whispering-gallery modes. *Phys. Lett. A* **137**, 393–397 (1989).

36. Gorodetsky, M. L. & Ilchenko, V. S. Optical microsphere resonators: optimal coupling to high-Q whispering-gallery modes. *J. Opt. Soc. Am. B* **16**, 147–154 (1999).

37. Ilchenko, V. S., Yao, X. S. & Maleki, L. Pigtailing the high-Q microsphere cavity: a simple fiber coupler for optical whispering-gallery modes. *Opt. Lett.* **24**, 723–725 (1999).

38. Treussart, F. *et al.* Microlasers based on silica microspheres. *Ann. Telecommun.* **52**, 557–568 (1997).

39. Serpenguzel, A., Arnold, S. & Griffel, G. Excitation of resonances of microspheres on an optical fiber. *Opt. Lett.* **20**, 654–656 (1995).

40. Knight, J. C., Cheung, G., Jacques, F. & Birks, T. A. Phase-matched excitation of whispering-gallery-mode resonances by a fiber taper. *Opt. Lett.* **22**, 1129–1131 (1997).

41. Cirac, J. I., van Enk, S. J., Zoller, P., Kimble, H. J. & Mabuchi, H. Quantum communication in a quantum network. *Physica Scripta* **T76**, 223–232 (1998).

42. Cai, M., Painter, O. & Vahala, K. J. Observation of critical coupling in a fiber taper to a silica-microsphere whispering-gallery mode system. *Phys. Rev. Lett.* **85**, 74–77 (2000).

43. Spillane, S. M., Kippenberg, T. J. & Vahala, K. J. Ultralow-threshold Raman laser using a spherical dielectric microcavity. *Nature* **415**, 621–623 (2002).

44. Purcell, E. M. Spontaneous emission probabilities at radio frequencies. *Phys. Rev.* **69**, 681–681 (1946).

45. Yamamoto, Y., Tassone, F. & Cao, H. *Semiconductor Cavity Quantum Electrodynamics* (Springer, New York, 2000).

46. Haroche, S. & Kleppner, D. Cavity quantum electrodynamics. *Phys. Today* **42**, 24–30 (1989).

47. Marzin, J. Y., Gerard, J. M., Izrael, A., Barrier, D. & Bastard, G. Photoluminescence of single Inas quantum dots obtained by self-organized growth on GaAs. *Phys. Rev. Lett.* **73**, 716–719 (1994).

48. Gerard, J. M. *et al.* Enhanced spontaneous emission by quantum boxes in a monolithic optical microcavity. *Phys. Rev. Lett.* **81**, 1110–1113 (1998).

49. Gerard, J. M. & Gayral, B. InAs quantum dots: artificial atoms for solid-state cavity-quantum electrodynamics. *Physica E* **9**, 131–139 (2001).

50. Gerard, J. M. *et al.* InAs quantum boxes in GaAs/AlAs pillar microcavities: From spectroscopic investigations to spontaneous emission control. *Physica E* **2**, 804–808 (1998).

51. Bayer, M. *et al.* Inhibition and enhancement of the spontaneous emission of quantum dots in structured microresonators. *Phys. Rev. Lett.* **86**, 3168–3171 (2001).

52. Gayral, B. *et al.* High-Q wet-etched GaAs microdisks containing InAs quantum boxes. *Appl. Phys. Lett.* **75**, 1908–1910 (1999).

53. Michler, P. *et al.* Quantum dot lasers using high-Q microdisk cavities. *Phys. Status Solidi B* **224**, 797–801 (2001).

54. Kiraz, A. *et al.* Cavity-quantum electrodynamics using a single InAs quantum dot in a microdisk structure. *Applied Phys. Lett.* **78**, 3932–3934 (2001).

55. Gerard, J. M. & Gayral, B. Strong Purcell effect for InAs quantum boxes in three-dimensional solid-state microcavities. *J. Lightwave Tech.* **17**, 2089–2095 (1999).

56. Pelton, M., Vuckovic, J., Solomon, G. S., Scherer, A. & Yamamoto, Y. Three-dimensionally confined modes in micropost microcavities: Quality factors and Purcell factors. *IEEE J. Quantum Elect.* **38**, 170–177 (2002).

57. Vuckovic, J., Pelton, M., Scherer, A. & Yamamoto, Y. Optimization of three-dimensional micropost microcavities for cavity quantum electrodynamics. *Phys. Rev. A* **66**, 023808 (2002).

58. Yablonovitch, E. Inhibited spontaneous emission in solid-state physics and electronics. *Phys. Rev. Lett.* **58**, 2059–2062 (1987).

59. Reese, C. *et al.* High-Q photonic crystal microcavities fabricated in a thin GaAs membrane. *J. Vac. Sci. Technol. B* **19**, 2749–2752 (2001).

60. Happ, T. D. *et al.* Enhanced light emission of InxGa1-xAs quantum dots in a two-dimensional photonic-crystal defect microcavity. *Phys. Rev. B* **66**, 041303 (2002).

61. Srinivasan, K. & Painter, O. Momentum space design of high-Q photonic crystal optical cavities. *Opt. Exp.* **10**, 670–684 (2002).

62. Srinivasan, K., Barclay, P., Painter, O., Chen, J., Cho, C. & Gmachl, C. Experimental demonstration of a high quality factor photonic crystal microcavity. *Appl. Phys. Lett.* (in the press).

63. Boroditsky, M. *et al.* Spontaneous emission extraction and Purcell enhancement from thin-film 2-D photonic crystals. *J. Lightwave Technol.* **17**, 2096–2112 (1999).

64. D. Bouwmeester, A. E. & A. Zeilinger . *The Physics of Quantum Information* (Springer, Berlin, 2000).

65. Kimble, H. J., Dagenais, M. & Mandel, L. Photon anti-bunching in resonance fluorescence. *Phys. Rev. Lett.* **39**, 691–695 (1977).

66. Basche, T., Moerner, W. E., Orrit, M. & Talon, H. Photon antibunching in the fluorescence of a single dye molecule trapped in a solid. *Phys. Rev. Lett.* **69**, 1516–1519 (1992).

67. Michler, P. *et al.* Quantum correlation among photons from a single quantum dot at room temperature. *Nature* **406**, 968–970 (2000).

68. Michler, P. *et al.* A quantum dot single-photon turnstile device. *Science* **290**, 2282–2285 (2000).

69. Santori, C., Pelton, M., Solomon, G., Dale, Y. & Yamamoto, E. Triggered single photons from a quantum dot. *Phys. Rev. Lett.* **86**, 1502–1505 (2001).

70. Zwiller, V. *et al.* Single quantum dots emit single photons at a time: Antibunching experiments. *Appl. Phys. Lett.* **78**, 2476–2478 (2001).

71. Thompson, R. M. *et al.* Single-photon emission from exciton complexes in individual quantum dots.

72. *Phys. Rev. B* **64**, 201302 (2001).

73. Lounis, B. & Moerner, W. E. Single photons on demand from a single molecule at room temperature. *Nature* **407**, 491–493 (2000).

74. Brunel, C., Lounis, B., Tamarat, P. & Orrit, M. Triggered source of single photons based on controlled single molecule fluorescence. *Phys. Rev. Lett.* **83**, 2722–2725 (1999).

75. Moreau, E. *et al.* Single-mode solid-state single photon source based on isolated quantum dots in pillar microcavities. *Appl. Phys. Lett.* **79**, 2865–2867 (2001).

76. Santori, C., Fattal, D., Vuckovic, J., Solomon, G. S. & Yamamoto, Y. Indistinguishable photons from a single-photon device. *Nature* **419**, 594–597 (2002).

77. Pelton, M. *et al.* Efficient source of single photons: A single quantum dot in a micropost microcavity. *Phys. Rev. Lett.* **89**, 233602 (2002).

78. Yuan, Z. L. *et al.* Electrically driven single-photon source. *Science* **295**, 102–105 (2002).

79. Qian, S. X., Snow, J. B., Tzeng, H. M. & Chang, R. K. Lasing droplets - highlighting the liquid-air interface by laser-emission. *Science* **231**, 486–488 (1986).

80. Lin, H. B., Eversole, J. D. & Campillo, A. J. Spectral properties of lasing microdroplets. *J. Opt. Soc. Am. B* **9**, 43–50 (1992).

81. Cai, M., Painter, O., Vahala, K. J. & Sercel, P. C. Fiber-coupled microsphere laser. *Opt. Lett.* **25**, 1430–1432 (2000).

82. Kuwatagonokami, M., Takeda, K., Yasuda, H. & Ema, K. Laser-emission from dye-doped polystyrene microsphere. *Japanese J. Appl. Phys. 2* **31**, L99–L101 (1992).

83. McCall, S. L., Levi, A. F. J., Slusher, R. E., Pearton, S. J. & Logan, R. A. Whispering-gallery mode microdisk lasers. *Appl. Phys. Lett.* **60**, 289–291 (1992).

84. Rex, N. B., Chang, R. K. & Guido, L. J. Threshold lowering in GaN micropillar lasers by means of spatially selective optical pumping. *IEEE Phot. Technol. Lett.* **13**, 1–3 (2001).

85. Deppe, D. G., Huffaker, D. L., Oh, T. H., Deng, H. Y. & Deng, Q. Low-threshold vertical-cavity surface-emitting lasers based on oxide-confinement and high contrast distributed Bragg reflectors. *IEEE J. Select. Top. Quantum Elect.* **3**, 893–904 (1997).

86. Sandoghdar, V. *et al.* Very low threshold whispering-gallery-mode microsphere laser. *Phys. Rev. A* **54**, R1777–R1780 (1996).

87. Macdougal, M. H., Dapkus, P. D., Pudikov, V., Zhao, H. M. & Yang, G. M. Ultralow threshold current vertical-cavity surface-emitting lasers with AlAs oxide-GaAs Distributed Bragg reflectors. *IEEE Phot. Technol. Lett.* **7**, 229–231 (1995).

88. Huffaker, D. L., Graham, L. A., Deng, H. & Deppe, D. G. Sub-40 microAmp continuous-wave lasing in an oxidized vertical-cavity surface-emitting laser with dielectric mirrors. *IEEE Phot. Technol. Lett.* **8**, 974–976 (1996).

89. Yamamoto, Y. & Slusher, R. E. Optical processes in microcavities. *Phys. Today* **46**, 66–73 (1993).

90. Rice, P. R. & Carmichael, H. J. Photon statistics of a cavity-QED laser - a comment on the laser-phase-transition analogy. *Phys. Rev. A* **50**, 4318–4329 (1994).

91. An, K. & Feld, M. A. Semiclassical four-level atom laser. *Phys. Rev. A* **56**, 1662–1665 (1997).

92. Graham, L. A., Huffaker, D. L., Csutak, S. M., Deng, Q. & Deppe, D. G. Spontaneous lifetime control of quantum dot emitters in apertured microcavities. *J. Appl. Phys.* **85**, 3383–3385 (1999).

93. Qian, S. X., Snow, J. B. & Chang, R. K. Coherent Raman mixing and coherent anti-Stokes Raman-scattering from individual micrometer-size droplets. *Opt. Lett.* **10**, 499–501 (1985).

94. Lin, H. B., Eversole, J. D. & Campillo, A. J. Continuous-wave stimulated Raman-scattering in microdroplets. *Opt. Lett.* **17**, 828–830 (1992).

95. Qian, S. X. & Chang, R. K. Multiorder Stokes emission from micrometer-size droplets. *Phys. Rev. Lett.* **56**, 926–929 (1986).

96. Zhang, J. Z., Chen, G. & Chang, R. K. Pumping of stimulated Raman-scattering by stimulated Brillouin-scattering within a single liquid droplet - input laser linewidth effects. *J. Opt. Soc. Am. B* **7**, 108–115 (1990).

97. Treussart, F. *et al.* Evidence for intrinsic Kerr bistability of high-Q microsphere resonators in superfluid helium. *Eur. Phys. J. D* **1**, 235–238 (1998).

98. Kaminow, I. P. & San, T. L. (eds) *Optical Fiber Telecommunications IV* (Academic Press, San Diego, 2002).

99. Alexander, S. B. *et al.* A precompetitive consortium on wide-band all-optical networks. *J. Lightwave Technol.* **11**, 714–735 (1993).

100. Hibino, Y., Maruno, T. & Okamoto, K. Recent progress on large-scale PLC technologies with advanced functions. *NTT Review* **13**, 4–9 (2001).

101. Kewitsch, A. S., Rakuljic, G. A., Willems, P. A. & Yariv, A. All-fiber zero-insertion-loss add-drop filter for wavelength- division multiplexing. *Opt. Lett.* **23**, 106–108 (1998).

102. Doerr, C. R. *et al.* 40-wavelength add-drop filter. *IEEE Phot. Technol. Lett.* **11**, 1437–1439 (1999).

103. Suzuki, S., Hatakeyama, Y., Kokubun, Y. & Chu, S. T. Precise control of wavelength channel spacing of microring resonator add-drop filter array. *J. Lightwave Technol.* **20**, 745–750 (2002).

104. Djordjev, K., Choi, S. J. & Dapkus, P. D. Microdisk tunable resonant filters and switches. *IEEE Phot. Technol. Lett.* **14**, 828–830 (2002).

105. Rabiei, P. Steier, W. H., Cheng Zhang and Dalton, L. R. Polymer micro-ring filters and modulators. *J. Lightwave Technol.* **20**, 1968–1975 (2002).

106. Little, B. E. *et al.* Wavelength switching and routing using absorption and resonance. *IEEE Phot. Technol. Lett.* **10**, 816–818 (1998).

107. Djordjev, K., Choi, S. J. & Dapkus, P. D. Vertically coupled InP microdisk switching devices with electroabsorptive active regions. *IEEE Phot. Technol. Lett.* **14**, 1115–1117 (2002).

108. Yariv, A. Critical coupling and its control in optical waveguide-ring resonator systems. *IEEE Phot. Technol. Lett.* **14**, 483–485 (2002).

109. Soref, R. A. & Little, B. E. Proposed N-wavelength M-fiber WDM crossconnect switch using active microring resonators. *IEEE Phot. Technol. Lett.* **10**, 1121–1123 (1998).

110. Chu, S. T. *et al.* An eight-channel add-drop filter using vertically coupled microring resonators over a cross grid. *IEEE Phot. Technol. Lett.* **11**, 691–693 (1999).

111. Grover, R. *et al.* Vertically coupled GaInAsP-InP microring resonators. *Opt. Lett.* **26**, 506–508 (2001).

112. Little, B. E. *et al.* Vertically coupled glass microring resonator channel dropping filters. *IEEE Phot. Technol. Lett.* **11**, 215–217 (1999).

113. Offrein, B. J. *et al.* Resonant coupler-based tunable add-after-drop filter in silicon-oxynitride technology for WDM networks. *IEEE J. Select. Top. Quantum Elect.* **5**, 1400–1406 (1999).

114. Little, B. E., Chu, S. T., Haus, H. A., Foresi, J. & Laine, J. P. Microring resonator channel dropping filters. *J. Lightwave Technol.* **15**, 998–1005 (1997).

114. Grover, R. *et al.* Parallel-cascaded semiconductor microring resonators for high- order and wide-FSR filters. *J. Lightwave Technol.* **20,** 872–877 (2002).

115. Yanagase, Y., Suzuki, S., Kokubun, Y. & Chu, S. T. Box-like filter response and expansion of FSR by a vertically triple coupled microring resonator filter. *J. Lightwave Technol.* **20,** 1525–1529 (2002).

116. Cooper, M. A. Optical biosensors in drug discovery. *Nat. Rev. Drug Discov.* 1, 515–527 (2002).

117. Marazuela, M. D. & Moreno-Bondi, M. C. Fiber-optic biosensors - an overview. *Anal. Bioanal. Chem.* **372,** 664–682 (2002).

118. Krioukov, E., Klunder, D. J. W., Driessen, A., Greve, J. & Otto, C. Sensor based on an integrated optical microcavity. *Opt. Lett.* **27,** 512–514 (2002).

119. Vollmer, F. *et al.* Protein detection by optical shift of a resonant microcavity. *Appl. Phys. Lett.* **80,** 4057–4059 (2002).

120. Walther, H. Quantum optics of a single atom. *Physica Scripta* **1,** 138–146 (1998)